Radiation-induced nitric oxide mitigates tumor hypoxia and radioresistance in a murine SCCVII tumor model

Masaki Nagane[a], Hironobu Yasui[a], Tohru Yamamori[a], Songji Zhao[b], Yuji Kuge[c], Nagara Tamaki[d], Hiromi Kameya[e], Hideo Nakamura[f], Hirotada Fujii[g], Osamu Inanami[a,*]

[a]Laboratory of Radiation Biology, Department of Environmental Veterinary Sciences, Graduate School of Veterinary Medicine, Hokkaido University, Sapporo, Japan

[b]Department of Tracer Kinetics and Bioanalysis, Graduate School of Medicine, Hokkaido University, Sapporo, Japan

[c]Central Institute of Isotope Science, Hokkaido University, Sapporo, Japan

[d]Department of Nuclear Medicine, Graduate School of Medicine, Hokkaido University, Sapporo, Japan

[e]Food Safety Division, National Food Research Institute, Tsukuba, Japan.

[f]Department of Chemistry, Hokkaido University of Education, Hakodate, Japan

[g] Department of Arts and Sciences, Center for Medical Education, Sapporo Medical University, Sapporo, Japan

Email address

Masaki Nagane: nagane@vetmed.hokudai.ac.jp

Hironobu Yasui: yassan@vetmed.hokudai.ac.jp

Tohru Yamamori: yamamorit@vetmed.hokudai.ac.jp

Songji Zhao: zsi@med.hokudai.ac.jp

Yuji Kuge: kuge@med.hokudai.ac.jp

Nagara Tamaki: natamaki@med.hokudai.ac.jp

Hiromi Kameya: kameya@affrc.go.jp

Hideo Nakamura: naka@science-edu.org

Hirotada Fujii: hgfujii@sapmed.ac.jp

Osamu Inanami: inanami@vetmed.hokudai.ac.jp

***Correspondence to:** Osamu Inanami, Laboratory of Radiation Biology, Department of Environmental Veterinary Sciences, Graduate School of Veterinary Medicine, Hokkaido University, Kita 18 Nishi 9, Kita-ku, Sapporo, Hokkaido 060-0818, Japan. Tel: (+81) 11-706-5235; Fax: (+81) 11-706-7373; E-mail: inanami@vetmed.hokudai.ac.jp

Running title: IR-induced NO regulates tumor hypoxia and radioresistance.

Abbreviations

3-NT, 3-nitrotyrosine; eNOS, endothelial nitric oxide synthase; ESR, electron spin resonance; H33342, Hoechst33342; iNOS, inducible nitric oxide synthase; LiNc-BuO, lithium 5,9,14,18,23,27,32,36-octa-*n*-butoxy-2,3-naphthalocyanine; L-NAME, N^G-nitro-L-arginine methyl ester; nNOS, neuronal nitric oxide synthase ;NO, nitric oxide; NOS, nitric oxide

synthase; pO_2, partial pressure of oxygen; positron emission tomography, PET.

ABSTRACT

Tumor hypoxia, which occurs mainly as a result of inadequate tissue perfusion in solid tumors, is a well-known challenge for successful radiotherapy. Recent evidence suggests that ionizing radiation (IR) upregulates nitric oxide (NO) production and that IR-induced NO has the potential to increase intratumoral circulation. However, the kinetics of NO production and the responsible isoforms for NO synthase in tumors exposed to IR remain unclear. In this study, we aimed to elucidate the mechanism by which IR stimulates NO production in tumors and the effect of IR-induced NO on tumor radiosensitivity. Hoechst33342 perfusion assay and electron spin resonance oxymetry showed that IR increased tissue perfusion and pO_2 in tumor tissue. Immunohistochemical analysis using two different hypoxic probes showed that IR decreased hypoxic regions in tumors; treatment with a nitric oxide synthase (NOS) inhibitor, L-NAME, abrogated the effects of IR. Moreover, IR increased endothelial NOS (eNOS) activity without affecting its mRNA or protein expression levels in SCCVII-transplanted tumors. Tumor growth delay assay showed that L-NAME decreased the anti-tumor effect of fractionated radiation (10 Gy × 2). These results suggested that IR increased eNOS activity and subsequent tissue perfusion in tumors. Increases in intratumoral circulation simultaneously decreased tumor hypoxia. As a result, IR-induced NO increased tumor radiosensitivity. Our study provides a new insight into the NO-dependent mechanism for efficient fractionated radiotherapy.

Keywords: ionizing radiation; tumor reoxygenation; electron spin resonance; nitric oxide.

Highlights

- IR-induced NO increased tissue perfusion and pO_2.
- IR increased NO production in tumors without changes in the mRNA and protein levels of NOS isoforms.
- NOS activity assay showed that IR upregulated eNOS activity in tumors.
- IR-induced NO decreased tumor hypoxia and altered tumor radiosensitivity.

INTRODUCTION

Low oxygen conditions drastically decrease cellular radiosensitivity and facilitate the adaptive survival responses of tumors [1]. Hence, tumor hypoxia in most solid tumors is a well-known obstacle for successful radiotherapy. It occurs mainly as a result of the excess proliferation of tumor cells and the accompanying deficiency in blood and nutrient supplies [1]. Recently, various strategies to overcome the low radiosensitivity in tumor hypoxia have been developed, such as hypoxic sensitizers, hyperbaric oxygen, and angiogenesis inhibitors [2].

A recent report demonstrated that treatment with nitric oxide (NO) donor (e.g. isosorbide dinitrate) increases both the partial pressure of oxygen (pO_2) in tissue and tumor radiosensitivity [3]. Thus, NO-mediated modulation of tumor blood flow could be a promising approach for improving cancer radiotherapy [4]. Meanwhile, several reports showed that ionizing radiation (IR) increases NO production and improves intratumoral circulation [5,6]. However, the NO synthase isoforms responsible for NO production in tumors exposed to IR remain uncertain. Sonveaux et al. demonstrated that IR increases endothelial nitric oxide synthase (eNOS) expression in tumor, leading to vasodilatation [5]. On the other hand, Li et al. reported that IR upregulates the expression level of inducible nitric oxide synthase (iNOS) and leads to the subsequent increase of angiogenesis in tumors [6].

Fractionated irradiation is one of the conventional therapeutic regimens in the clinical setting and is known to utilize the reoxygenation effect. In 1972, Kallman proposed that IR reoxygenates hypoxic regions in tumors and decreases radioresistance [7]. However, the involvement of IR-induced NO in the reoxygenation of hypoxic regions has not been elucidated.

It is extremely important to clarify the duration in which IR-induced NO has an influence on tumor reoxygenation, which is considered to be associated with radiosensitivity in tumors treated with fractionated irradiation.

We conducted this study to elucidate the mechanism by which IR stimulates NO production in tumors and the effect of IR-induced NO on tumor radiosensitivity. For this purpose, we employed immunohistochemistry and *in vivo* electron spin resonance (ESR) spectroscopy to trace the spatiotemporal changes of the tumor oxygenation status in murine SCCVII tumors exposed to IR. In addition, we evaluated nitric oxide synthase (NOS) expression and activity in tumors after IR to determine the source of IR-induced NO production.

MATERIALS AND METHODS

Tumor model and irradiation

Female C3H mice aged 6 weeks were purchased from Japan SLC (Hamamatsu, Japan). SCCVII cells, a squamous carcinoma cell line derived from C3H mice, were maintained *in vitro* in Eagle's minimum essential medium containing 10% fetal bovine serum. For allograft transplantation, SCCVII cells were inoculated subcutaneously into hind legs of mice (5.0×10^6 cells/head). Tumor volume was calculated as tumor volume = $\pi/6 \times a \times b \times c$, where a, b, and c are the orthogonal dimensions of the tumor.

Anesthetized tumor-bearing mice (tumor size; 400–500 mm^3) were X-ray-irradiated at a dose of 10 or 13 Gy using a PANTAK HF-350 X-ray generator (Shimadzu, Kyoto, Japan) at a dose rate of 0.85 Gy/min (0.5 mm Cu and 0.5 mm Al filter, 200 kVp, 20 mA). The mice were X-irradiated locally by lead-shielding the whole body except the tumor. For *in vivo* experiments, N^G-nitro-L-arginine methyl ester (L-NAME; DOJINDO, Kumamoto, Japan) was intraperitoneally injected into tumor-bearing mice at 30 mg/kg at 30 min before irradiation, followed by *ad lib* administration in drinking water at a concentration of 500 mg/L [8].

All animal experiments were performed according to the established guidelines of the "Law for The Care and Welfare of Animals in Japan", and approved by the Animal Experiment Committee of the Graduate School of Veterinary Medicine, Hokkaido University.

In vivo ESR oxymetry

An oxygen-sensitive probe, lithium 5,9,14,18,23,27,32,36-octa-*n*-butoxy-2,3-naphthalocyanine

(LiNc-BuO) was prepared according to a previous report [9]. *In vivo* ESR oxymetry was performed as described elsewhere [10]. In brief, LiNc-BuO suspension was implanted in tumors (200 μg/mouse in 20 μl PBS containing 5% dextran) and mice were left for longer than 24 h before ESR measurement. The ESR spectra of LiNc-BuO were recorded using a JES-TE200 continuous-wave L-band ESR spectrometer with a surface-coil resonator (JEOL, Tokyo, Japan). Single-scan ESR spectra were obtained from LiNc-BuO implanted in tumors with the following parameters: scan time 480 s, field scanning 1.0 mT, field modulation 0.032 mT, time constant 10 s, microwave frequency 1.096 GHz, and microwave power 3.12 mW. The linewidths of the obtained spectra were converted into pO_2 values according to the calibration curve of LiNc-BuO probes prepared before animal experiments.

Immunohistochemistry

Pimonidazole (Hypoxyprobe-1 Kit; Hypoxyprobe, Inc., Burlington, MA) was intravenously administered to tumor-bearing mice at 1 h before IR to label the region of primarily existing hypoxia. EF5 (supplied by Dr. C. J. Koch [11]) was then administered to mice at 23 h or 47 h after IR to label the region of altered hypoxia. Tumor tissues were excised at 1 h after EF5 injection, fixed with 4% buffered formaldehyde, embedded in paraffin, and sectioned at 3-μm thick. After antigen retrieval and blocking of non-specific binding, slides were probed with monoclonal anti-EF5 (1:10) or anti-pimonidazole (1:200) antibodies. The slides were then incubated with Alexa Fluor 594 anti-mouse or Alexa Fluor 488 anti-rabbit IgG (both 1:2000, Invitrogen, Carlsbad, CA) secondary antibodies, respectively.

Images of ten fields from each sample were acquired at ×100 magnification using a fluorescence microscope (BX61; Olympus, Tokyo, Japan) equipped with a digital camera (DP71; Olympus), and the pixel number of the pimonidazole- or EF5-positive areas in each image was quantified using ImageJ software (National Institutes of Health, MD, USA). To evaluate the change in tumor hypoxia, the ratio of the pixel number of EF5-positive areas to that of the pimonidazole-positive areas was calculated.

Analysis of tissue perfusion in tumors

The status of tissue perfusion in tumors after IR was evaluated by the administration of Hoechst 33342 (H33342; DOJINDO, Kumamoto, Japan) as an exogenous perfusion marker [12]. The H33342 signals in the frozen sections were recorded and analyzed as described above. To perform quantitative analysis, the pixel number of H33342-positive areas were divided by that of the total tumor area and expressed as the perfusion area (%).

Western blotting

Western blot analyses for 3-nitrotyrosine (3-NT), iNOS, eNOS, and CD31, cyclooxygenase-2 (Cox-2), were performed according to a previous report [13]. Proteins separated by SDS-PAGE were transferred to a nitrocellulose membrane (ADVANTEC Toyo, Tokyo, Japan). Membranes were probed with antibodies against 3-NT, iNOS, eNOS, CD31 (Abcam, Cambridge, UK), and Cox-2 (Santa Cruz Biotechnology, Santa Cruz, CA) and subsequent HRP-conjugated secondary antibodies.

RT-PCR analysis

Total RNA from the excised tumors was isolated using a SV Total RNA Isolation system (Promega Corporation, Madison, WI) according to the manufacturer's instructions. Two micrograms of RNA were reverse-transcribed using ReverTra Ace qPCR RT Master Mix (TOYOBO, Osaka, Japan). Real-time PCR analysis was performed by a LightCycler Nano System together with FastStart Essential DNA Green Master (Roche Applied Science, Mannheim, Germany). The specific primer sequences for PCR were as follows: for neural NOS (nNOS), 5'-CAAGAACTGGGAGACAGATG-3' and 5'- CTGACTTCCGTATGTGATGG-3'; for iNOS, 5'-GACCTGAAAGAGGAAAAGGA-3' and 5'-TGTATTGTTGGGCTGAGAAC-3'; for eNOS, 5'-AAAGCTGCAGGTATTTGATG-3' and 5'-TGCCTCTATTTGTTGCGTAT-3'; for β_2-microglobulin (β2M), 5'-AGGAGTGGATCTCTGGAAAG -3' and 5'-GCTTGATCACATGTCTCGAT-3'. The PCR conditions were set as follows: 95°C for 10 min, followed by 45 cycles of 95°C for 20 s, 60°C for 20 s, and 72°C for 20 s. The fluorescence intensity was measured at the end of every extension phase. Relative mRNA levels of NOS isoforms were normalized by that of β2M set as an internal control. Melting curve analyses were performed using fluorescence data acquired by integrating the signal during a liner temperature transition of 60°C to 95°C at 0.1°C/sec.

NOS activity assay

NOS activity was measured using a NOS Activity Assay Kit (Abnova, Taipei, Taiwan)

according to the manufacturer's instructions. This assay is based on the conversion of [^{14}C] L-arginine to [^{14}C] L-citrulline by NOS. NOS activity was calculated as follows: NOS activity (pmol/μg/min) = [^{14}C]-radioactivity in the flow-through (CPM)/total protein amount (μg)/specific radioactivity of [^{14}C] L-arginine (Bq/pmol). To measure eNOS activity, we performed the assays in the presence or absence of a general NOS inhibitor, L-NAME, or an iNOS selective inhibitor, 1400W (Wako Pure Chemical Industries, Osaka, Japan).

Statistical analysis

All values are expressed as means ± S.E. of three to eight independent experiments. Differences between groups were evaluated by Student's t-test (two-sided) and considered to be significant at $P<0.05$.

RESULTS

Radiation-induced NO modulates tumor oxygenation status

To perform a detailed analysis of the temporal changes in tumor oxygenation status after IR, we employed *in vivo* ESR oxymetry, which allowed us to measure tumor pO_2 continuously. ESR oxymetry showed that IR induced a rapid increase in tumor pO_2 from 4.3 mmHg to 17.4 mmHg at 24 h. After the first reoxygenation, tumor pO_2 decreased to 7.7 mmHg at 48 h after irradiation and remained elevated up to 120 h (Fig. 1A). Moreover, L-NAME treatment inhibited the early increase of pO_2 after IR, whereas the late plateau phase from 48 h was not affected (Fig. 1A). These results indicated that IR-induced NO was involved in the increase in tissue pO_2 at 12 h and 24 h after IR.

Next, to clarify the spatiotemporal changes of tumor hypoxia, we performed an immunohistochemical analysis using two hypoxia probes, pimonidazole and EF5. To this end, these two probes were separately injected into mice before and after irradiation, with the aim of labeling two different hypoxic regions; the first probe, pimonidazole, accumulates to the pre-existing hypoxic regions, and the second probe, EF5, accumulates to the newly-emerged hypoxic regions after IR. As shown in Figure 1B, we found a similar level of pimonidazole accumulation in all groups, indicating that the extent of tumor hypoxia before IR was almost equal. When EF5 was injected 1 h after pimonidazole administration, the complete colocalization of these probes in the tumors was observed (Fig. 1B; left). When transplanted tumors were irradiated at 1 h after pimonidazole injection, followed by EF5 injection at 24 h after IR, the EF5-positive regions were reduced compared to the pimonidazole-positive regions

(Fig. 1B; middle). At 48 h after IR, the EF5-positive regions reemerged and partly overlapped with the pimonidazole-positive regions (Fig. 1B; right). In addition, we performed positron emission tomography (PET) scanning using [^{18}F]-FMISO as a radiolabeled hypoxia marker. In tumors at 24 h after 13 Gy X-irradiation, PET images showed that the uptake of [^{18}F]-FMISO was diminished after irradiation (Supplementary Fig. 1A). Similarly, the autoradiographs for [^{18}F]-FMISO in the tumor cryosections showed a reduction in hypoxic regions after irradiation (Supplementary Figs. 1B and 1C). Changes in tumor volumes were hardly observed within 24 h after X-irradiation (Supplementary Fig. 1D). These results indicated that X-irradiation induced tumor reoxygenation without affecting tumor size.

While IR induced a substantial decrease in EF5-positive areas at 24 h after IR in the absence of L-NAME (Fig. 1B), L-NAME treatment clearly prevented it (Fig. 1C; middle). Quantitative analysis showed significant decreases in the EF5/pimonidazole fraction ratio at 24 h and 48 h after IR (13.1% and 58.2% of pimonidazole-positive fractions, respectively) (Fig. 1D). In the presence of L-NAME, IR resulted in a gradual reduction of the EF5/pimonidazole fraction ratio up to 48 h after irradiation (78.7% at 24 h and 56.4% at 48 h) (Fig. 1D). It was significantly different from the change in the EF5/pimonidazole fraction ratio after irradiation without L-NAME (Fig. 1D), suggesting the involvement of IR-induced NO in the tumor reoxygenation.

Radiation-induced NO increases intratumoral circulation

Several reports have demonstrated that IR-induced NO production is associated with an increase

in intratumoral blood circulation and tissue perfusion via vasodilation [4,14]. We thus performed a H33342 perfusion assay to evaluate the blood supply to tumor tissues after IR (13 Gy). As shown in Figure 2A, the perfused areas were increased after irradiation, indicating that IR enhanced blood supply in the tumors. Quantitative analysis showed that the perfused areas in tumors at 24 and 48 h after IR (30.9% and 31.3%, respectively) were three times larger than those in the nonirradiated control (8.5%) (Fig. 2B).

To investigate the involvement of NO in the IR-induced tissue perfusion, we tested the effect of L-NAME. Administration of L-NAME completely inhibited the increase of the perfused area by IR at 24 h, but this inhibition disappeared at 48 h (24.5%) (Fig. 2B). To clarify whether IR stimulates NO production in tumors, we examined the protein nitration levels after IR by western blotting for 3-NT [15]. Figure 2C shows that several bands of nitrated protein (indicated by arrows) were increased in X-irradiated tumors, suggesting that IR induced NO production. We also tested the effect of L-NAME on NO production in X-irradiated tumors and found that the administration of L-NAME to tumor-bearing mice at 30 min before IR abolished the increase in 3-NT levels at 24 h after irradiation (Fig.2C).

IR increases eNOS activity in SCCVII tumors

To determine the source of IR-induced NO, we next evaluated the mRNA and protein

expression levels of the NOS isoforms (nNOS, iNOS, and eNOS). RT-PCR analysis revealed that the mRNA levels of each NOS isoform were not changed after IR (Fig.3A). In addition, nNOS mRNA was hardly detectable in SCCVII tumors (nNOS mRNA in nonirradiated tumor; Cq = 0.009 ± 0.001, irradiated tumor; Cq = 0.011 ± 0.003). This result led us to exclude nNOS from further analysis. As shown in Figure 3B, western blot analysis showed that IR did not increase the protein expression levels of iNOS and eNOS. Furthermore, we observed no difference in the protein expression levels of CD31 and Cox-2 between control and X-irradiated tumors, suggesting that neither angiogenesis nor inflammation had occurred at 18 h after IR (Fig. 3B). We then tested the enzymatic activities of NOS in tumor-tissue extracts with or without IR. It showed that IR increased NOS activity in tumors (Fig. 3C; DMSO [1%]). These results suggested that NO production in X-irradiated tumors was not due to altered NOS protein expression, but to increased enzymatic activity of either iNOS or eNOS.

To determine which NOS isoform plays a role in NO production after IR, we evaluated the effect of a general NOS inhibitor, L-NAME, and an iNOS-specific inhibitor, 1400W, on NOS activity using protein extracts from SCCVII tumors. While L-NAME treatment significantly inhibited IR-induced upregulation of NOS activity, 1400W did not (Fig. 3C). These results indicated that eNOS but not iNOS was responsible for NOS activation in irradiated tumors.

Radiation-induced NO increases tumor radiosensitivity

The hypoxic region in tumors is an important factor to determine the efficacy of radiation

therapy. Because radiation-induced NO decreased tumor hypoxia at 12 h and 24 h after IR (Fig. 1), we evaluated the effect of radiation-induced NO on tumor growth after fractionated irradiation. Tumor growth delay assay showed that the fractionated irradiation at intervals of 18 h (10 Gy × 2) clearly decreased tumor growth rate (Fig. 4). To examine the effect of L-NAME on this anti-tumor effect, tumor-bearing mice were treated with L-NAME after the first irradiation until the second irradiation. As a result, we found that L-NAME significantly diminished the anti-tumor effect caused by the fractionated irradiation (Fig. 4).

DISCUSSION

We conducted this study to elucidate the mechanism by which IR stimulates NO production in tumors and the effect of IR-induced NO on tumor radiosensitivity. To evaluate the effect of IR-induced NO on tissue pO_2, hypoxic regions in tumors, and intratumoral circulation, we performed a series of experiments to detect spatiotemporal microenvironmental changes. Firstly, continuous measurement for pO_2 by ESR oxymetry with LiNc-BuO showed the two-phasic tumor reoxygenation after IR consisted of an early phase (12 h to 24 h) and a late phase (48 h to 120 h) (Fig. 1A). Secondly, hypoxic regions were decreased in tumors at 24 h and 48 h after IR (Figs. 1B and 1D). Finally, accompanied by the changes in tissue pO_2 and hypoxia after IR, H33342 perfusion assay demonstrated a sustained increase in intratumoral circulation for 24 h and 48 h after IR (Figs. 2A and 2B). Importantly, at both phases, we did not observe a significant induction of tumor shrinkage (Supplementary Fig. 1) and angiogenesis (data not shown) that might contribute to the tumor oxygenation status. These results suggested that the IR increased blood diffusion from the vessels leading to tumor reoxygenation. In support of this hypothesis, Fokas et al. recently demonstrated that tumor pO_2 change is partly due to the increase in blood diffusion after IR [17].

To investigate the involvement of IR-induced NO in the changes in tissue perfusion, tissue pO_2, and tumor hypoxia, we tested the effect of L-NAME. L-NAME treatment significantly inhibited the early increases of perfusion and pO_2 after IR (Figs. 1 and 2). Crokart et al. proposed that IR-induced inflammation is involved in the increase in tumor pO_2, based on their observation that an anti-inflammation drug diclofenac partly inhibited the reoxygenation

[18]. However, as shown in Figure 3B, we did not observe an increase in an inflammation marker, Cox-2, suggesting that IR-induced inflammation did not occur in these experimental conditions.

Although IR increased protein nitration, the mRNA and protein levels of NOS isoforms did not change after IR (Figs. 2C and 3AB). In addition, the IR-induced increase in NOS activity was inhibited by a general NOS inhibitor L-NAME, but not by an iNOS-specific inhibitor, 1400W (Fig. 3C). We confirmed that this concentration of 1400W completely inhibited iNOS activity purified from murine macrophages (data not shown). Moreover, RT-PCR analysis showed that nNOS was poorly expressed in SCCVII tumors (Fig 3B). These results suggested that eNOS is responsible for IR-induced NO production. At present, it remains unclear how IR triggers eNOS activation in vascular endothelial cells. Since the phosphorylation of eNOS is known to be important in the regulation of its activity, further examination of its phosphorylation mechanism is required to understand IR-induced reoxygenation in solid tumors.

In conclusion, the present study demonstrated that IR stimulated NO production via the activation of eNOS, leading to a reduction in hypoxic regions in tumors. Importantly, L-NAME treatment attenuated the anti-tumor effect of the fractionated radiation (10 Gy x 2) *in vivo*. These results suggested that the first round of IR decreases hypoxic regions in tumors through eNOS upregulation, leading to an increase in tumor radiosensitivity against the second IR round. These findings may provide new insights for the development of effective radiation therapy for solid tumors.

Acknowledgments- This work was supported in part by JSPS KAKENHI (Grant Numbers, 24659551 [OI], 23780286 [TY], and 23791375 [HY], 25861045 [HY]), Takeda Science Foundation [TY], and The Akiyama Life Science Foundation [HY]. The authors thank Professor Cameron Koch (Radiation Oncology, University of Pennsylvania, PA) and the National Cancer Institute (Bethesda, MD) for providing EF5.

REFERENCES

[1] E.J. Hall, A.J. Giaccia, Radiobiology for the Radiologist, 7th ed., Lippincott Williams & Wilkins, Philadelphia (PA), 2011.

[2] W.R. Wilson, M.P. Hay, Targeting hypoxia in cancer therapy, Nat Rev Cancer 11 (2011) 393-410.

[3] B.F. Jordan, P. Sonveaux, O. Feron, V. Grégoire, N. Beghein, C. Dessy, B. Gallez, Nitric oxide as a radiosensitizer: evidence for an intrinsic role in addition to its effect on oxygen delivery and consumption, Int J Cancer 109 (2004) 768-773.

[4] P. Sonveaux, B.F. Jordan, B. Gallez, O. Feron, Nitric oxide delivery to cancer: why and how?, Eur J Cancer 45 (2009) 1352-1369.

[5] P. Sonveaux, C. Dessy, A. Brouet, B.F. Jordan, V. Grégoire, B. Gallez, J.L. Balligand, O. Feron, Modulation of the tumor vasculature functionality by ionizing radiation accounts for tumor radiosensitization and promotes gene delivery., FASEB J 16 (2002) 1979-1981.

[6] F. Li, P. Sonveaux, Z.N. Rabbani, S. Liu, B. Yan, Q. Huang, Z. Vujaskovic, M.W. Dewhirst, C.Y. Li, Regulation of HIF-1alpha stability through S-nitrosylation, Mol Cell 26 (2007)

63-74.

[7] R.F. Kallman, The Phenomenon of Reoxygenation and Its Implications for Fractionated Radiotherapy, Radiology 105 (2012) 135-142.

[8] G.A. Gray, C. Schott, G. Julou-Schaeffer, I. Fleming, J.R. Parratt, J.C. Stoclet, The effect of inhibitors of the L-arginine/nitric oxide pathway on endotoxin-induced loss of vascular responsiveness in anaesthetized rats., Br J Pharmacol 103 (1991) 1218-1224.

[9] R.P. Pandian, N.L. Parinandi, G. Ilangovan, J.L. Zweier, P. Kuppusamy, Novel particulate spin probe for targeted determination of oxygen in cells and tissues., Free Radic Biol Med 35 (2003) 1138-1148.

[10] H. Fujii, K. Sakata, Y. Katsumata, R. Sato, M. Kinouchi, M. Someya, S. Masunaga, M. Hareyama, H.M. Swartz, H. Hirata, Tissue oxygenation in a murine SCC VII tumor after X-ray irradiation as determined by EPR spectroscopy., Radiother Oncol 86 (2008) 354-360.

[11] E.M. Lord, L. Harwell, C.J. Koch, Detection of hypoxic cells by monoclonal antibody recognizing 2-nitroimidazole adducts, Cancer Res 53 (1993) 5721-5726.

[12] H. Kobayashi, K. Reijnders, S. English, A.T. Yordanov, D.E. Milenic, A.L. Sowers, D.

Citrin, M.C. Krishna, T.A. Waldmann, J.B. Mitchell, M.W. Brechbiel, Application of a macromolecular contrast agent for detection of alterations of tumor vessel permeability induced by radiation., Clin Cancer Res 10 (2004) 7712-7720.

[13] D.T. Hess, A. Matsumoto, S.O. Kim, H.E. Marshall, J.S. Stamler, Protein S-nitrosylation: purview and parameters., Nat Rev Mol Cell Biol 6 (2005) 150-166.

[14] P. Sonveaux, A. Brouet, X. Havaux, V. Grégoire, C. Dessy, J.L. Balligand, O. Feron, Irradiation-induced angiogenesis through the up-regulation of the nitric oxide pathway: implications for tumor radiotherapy, Cancer Res 63 (2003) 1012-1019.

[15] P. Pacher, J.S. Beckman, L. Liaudet, Nitric oxide and peroxynitrite in health and disease, Physiol Rev 87 (2007) 315-424.

[16] L.M. van Putten, Tumour reoxygenation during fractionated radiotherapy; studies with a transplantable mouse osteosarcoma., Eur J Cancer 4 (1968) 172-182.

[17] E. Fokas, J. Hänze, F. Kamlah, B.G. Eul, N. Lang, B. Keil, J.T. Heverhagen, R. Engenhart-Cabillic, H. An, F. Rose, Irradiation-dependent effects on tumor perfusion and endogenous and exogenous hypoxia markers in an A549 xenograft model., Int J Radiat Oncol Biol Phys 77 (2010) 1500-1508.

[18] N. Crokart, B.F. Jordan, C. Baudelet, R. Ansiaux, P. Sonveaux, V. Grégoire, N. Beghein, J. DeWever, C. Bouzin, O. Feron, B. Gallez, Early reoxygenation in tumors after irradiation: determining factors and consequences for radiotherapy regimens using daily multiple fractions., Int J Radiat Oncol Biol Phys 63 (2005) 901-910.

[19] P. Sonveaux, F. Frérart, C. Bouzin, A. Brouet, J. Dewever, B.F. Jordan, B. Gallez, O. Feron, Irradiation promotes Akt-targeting therapeutic gene delivery to the tumor vasculature, Int J Radiat Oncol Biol Phys 67 (2007) 1155-1162.

[20] R. Rafikov, F.V. Fonseca, S. Kumar, D. Pardo, C. Darragh, S. Elms, D. Fulton, S.M. Black, eNOS activation and NO function: structural motifs responsible for the posttranslational control of endothelial nitric oxide synthase activity, J Endocrinol 210 (2011) 271-284.

FIGURE LEGENDS

Figure 1. IR-induced NO production increased tissue pO_2 and decreased hypoxic regions in tumors. LiNc-BuO crystals were implanted in SCCVII and tumor pO_2 was measured continuously up to 120 h after IR. (A) Changes in tumor pO_2 in SCCVII after IR. White circles, 4 Gy; white squares, 13 Gy without L-NAME; black squares, 13 Gy with L-NAME. (B) Representative images of tumor hypoxia before and after IR. Pimonidazole (green) represented the hypoxic regions before IR, whereas EF5 (red) detected the hypoxic regions at 24 and 48 h after IR. White arrows indicate new hypoxic regions. Bar = 200 μm. (C) Representative images of tumor hypoxia before and after IR in L-NAME-treated mice. (D) The EF5/pimonidazole ratio was obtained by calculating the proportions of hypoxic regions labeled with pimonidazole and those labeled with EF5. Bar = 200 μm. Error bars represent S.E. $^{**}P<0.01$ *vs.* nonirradiated control.

Figure 2. IR-induced NO production increased tissue perfusion in tumors. (A) Vascular perfusion depicted by the diffusion of H33342 in X-irradiated SCCVII tumors treated with and without L-NAME. Tumor-bearing mice were intravenously injected with H33342 at 4 min before sacrifice. Bar = 200 μm. (B) Quantitative data obtained by H33342 perfusion assay (black square, no drug; white squares, L-NAME). Error bars represent S.E. $^{**}P<0.01$ *vs.* X-irradiated tumors without L-NAME. (C) Representative images of western blotting for 3-NT. Mice were divided into three groups: control (Nonirradiated), IR only (13 Gy, 24 h), and IR + L-NAME (13 Gy with L-NAME, 24 h).

Figure 3. IR increased protein nitration and eNOS activity in tumors. (A) Changes in mRNA expression of nNOS, iNOS, and eNOS after IR (10 Gy, 18 h). (B) Representative images of western blotting for iNOS, COX-2, eNOS, and CD31. (C) NOS activity assay with general NOS inhibitor (L-NAME, 20 mM) and iNOS selective inhibitor (1400W, 10 μM). Error bars represent S.E. $^{*}P<0.05$ *vs.* nonirradiated tumor. $^{\#}P<0.05$ *vs.* L-NAME.

Figure 4. NO-induced tumor reoxygenation increased radiosensitivity. Growth delay assay after IR (white square, 0 Gy without L-NAME; black squares, 0 Gy with L-NAME; white triangle, 10 Gy × 2 without L-NAME; black triangle, 10 Gy × 2 with L-NAME). Error bars represent S.E. $*P<0.05$ *vs.* 10 Gy × 2 without L-NAME.

SUPPLEMENTARY MATERIALS AND METHODS

[^{18}F]-FMISO imaging

[^{18}F]-FMISO (18.5 MBq/head) was intravenously injected into mice at 21 h after X-irradiation. At 3 h after [^{18}F]-FMISO injection, the anesthetized mice were placed in a small animal PET scanner (Inveon; Siemens Medical Solutions USA Inc., Knoxville, TN) in a prone position. Dynamic PET (list-mode acquisition) imaging was performed for 20 min, followed by computed tomography (CT) imaging for the acquisition of anatomical information. The data were reconstructed and corrected for attenuation and scatter using 2-D filtered backprojection. The image matrix was 256 × 256 × 159, resulting in a voxel size of 0.385 × 0.385 × 0.796 mm. The standardized uptake value (SUV) was calculated using the single maximum pixel count within the region of interest and normalized to the injected dose and mouse body weight. After PET/CT imaging, mice were killed and fresh frozen tumor sections were obtained. The cryosections were exposed to a phosphor imaging plate cassette, together with a set of calibrated standards, and overnight autoradiography (ARG) exposure was performed to detect the distribution of [^{18}F]-FMISO. ARG images were analyzed using a computerized imaging analysis system (FLA 7000; Fuji Film Co. Ltd., Tokyo, Japan).

SUPPLEMENTARY FIGURE LEGENDS

Supplementary Figure 1. [^{18}F]-FMISO imaging for the detection of tumor reoxygenation.

(A) Representative images of [^{18}F]-FMISO PET/CT in a nonirradiated tumor (left) and one

exposed to 13 Gy of X-rays (13 Gy, right) (Top, coronal plane; middle, transverse plane; bottom, sagittal plane). (B) Representative images of [^{18}F]-FMISO ARG in nonirradiated (left) and X-rayed (13 Gy, right) tumors (T, tumor; M, skeletal muscle). (C) Quantitative data obtained by [^{18}F]-FMISO ARG (black square, nonirradiated; white squares, 13 Gy). Error bars represent S.E. $^{**}P<0.01$ *vs.* X-irradiated tumor without L-NAME. (D) Tumor volume measured before [^{18}F]-FMISO injection. Error bars represent S.E. $^{*}P<0.05$ *vs.* a nonirradiated control.

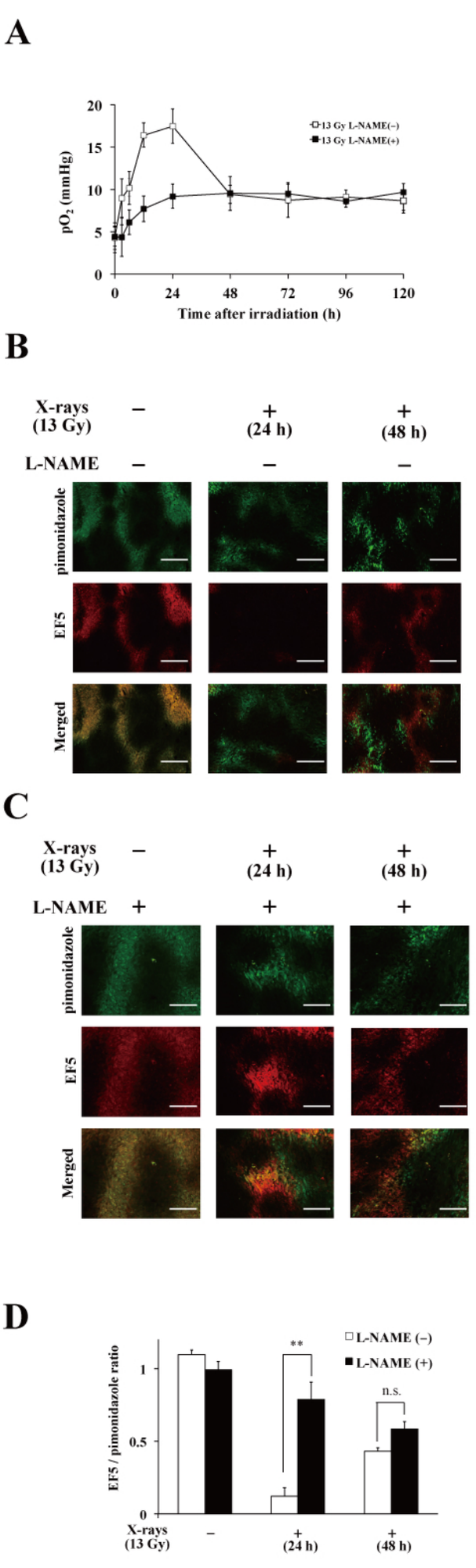

Fig. 1 Nagane *et al.*

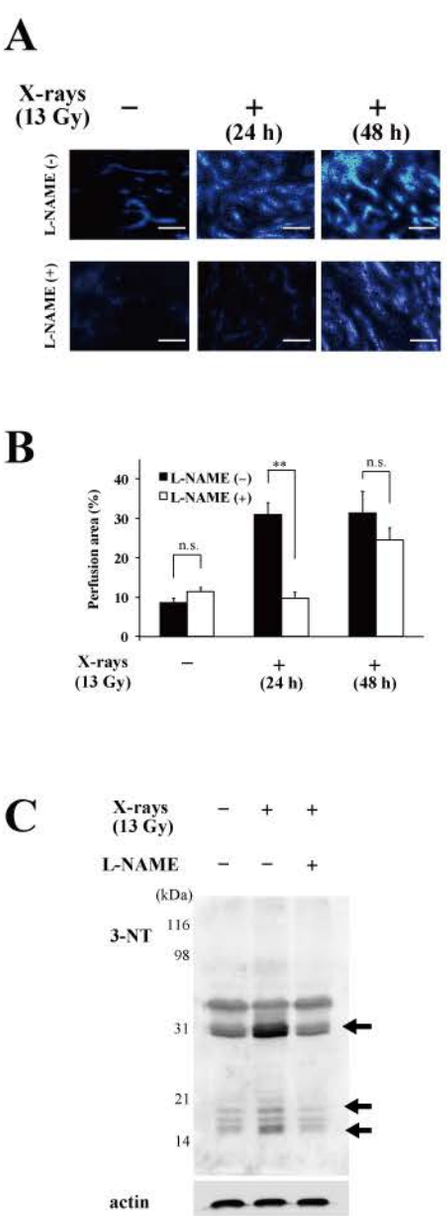

Fig. 2 Nagane *et al.*

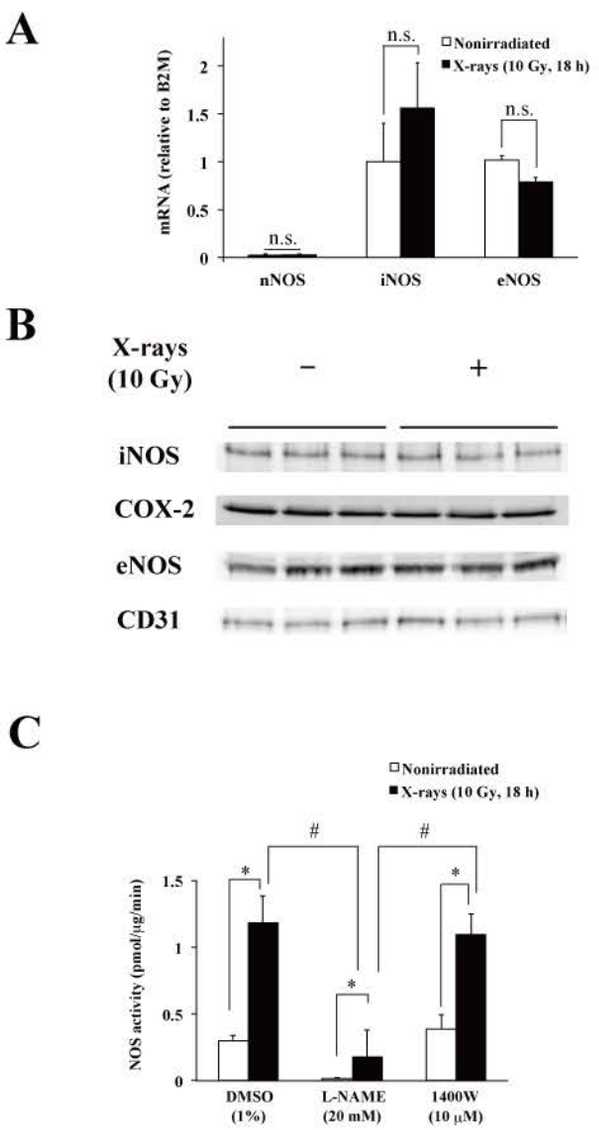

Fig. 3. Nagane *et al.*

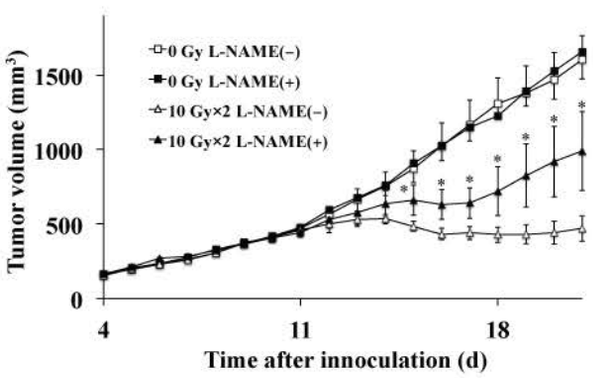

Fig. 4. Nagane *et al.*

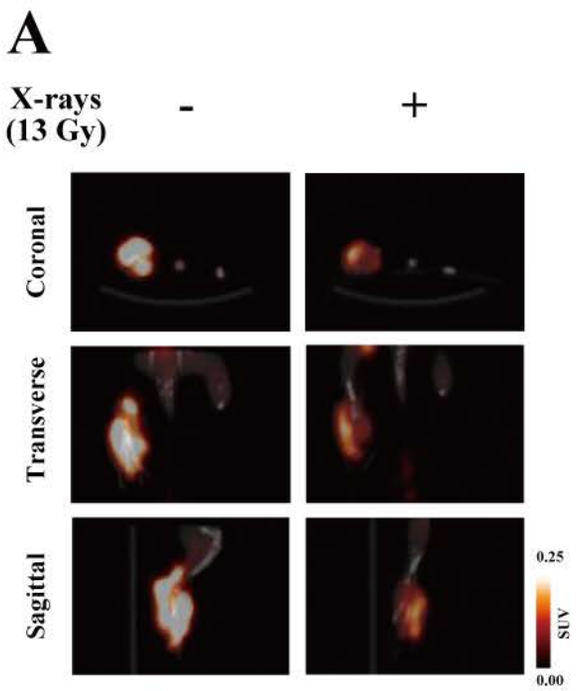

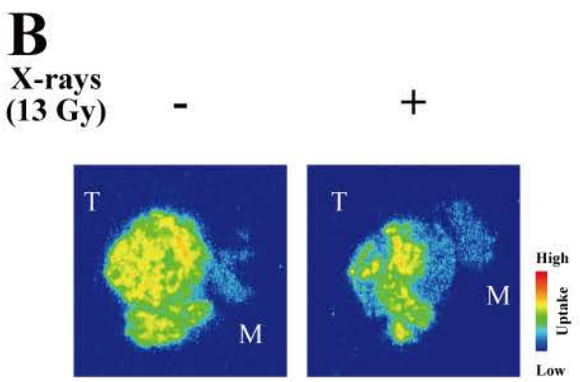

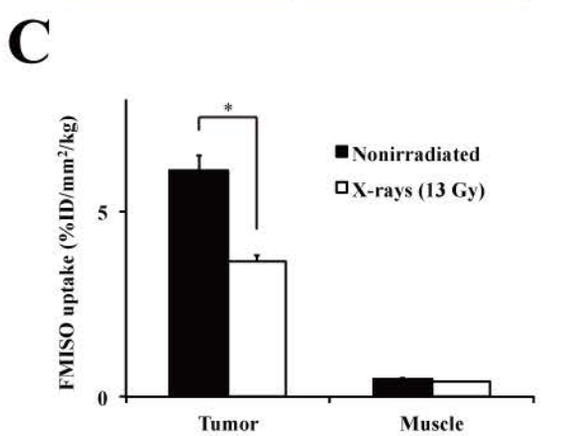

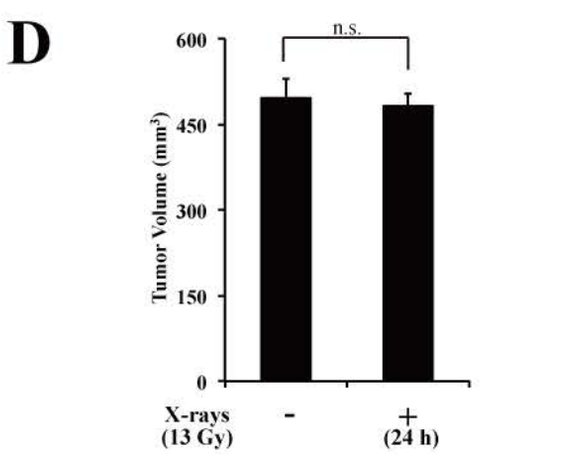

Supplementary Fig. 1 Nagane *et al.*